Classification of brain tumor extracts by high resolution 1H MRS using partial least squares discriminant analysis

A.V. Faria, F.C. Macedo Jr., A.J. Marsaioli, M.M.C. Ferreira and F. Cendes

Classification of brain tumor extracts by high resolution ^{1}H MRS using partial least squares discriminant analysis

A.V. Faria[1,3], F.C. Macedo Jr.[4,5], A.J. Marsaioli[4],
M.M.C. Ferreira[4] and F. Cendes[2]

[1]Departamento de Radiologia, [2]Departamento de Neurologia, Faculdade de Ciências Médicas,
Universidade Estadual de Campinas, Campinas, SP, Brasil
[3]The Russell H. Morgan Department of Radiology and Radiological Science, School of Medicine,
The Johns Hopkins University, Baltimore, MD, USA
[4]Instituto de Química, Universidade Estadual de Campinas, Campinas, SP, Brasil
[5]Departamento de Química, Centro de Ciências Exatas, Universidade Estadual de Londrina,
Londrina, PR, Brasil

Abstract

High resolution proton nuclear magnetic resonance spectroscopy (^{1}H MRS) can be used to detect biochemical changes *in vitro* caused by distinct pathologies. It can reveal distinct metabolic profiles of brain tumors although the accurate analysis and classification of different spectra remains a challenge. In this study, the pattern recognition method partial least squares discriminant analysis (PLS-DA) was used to classify 11.7 T ^{1}H MRS spectra of brain tissue extracts from patients with brain tumors into four classes (high-grade neuroglial, low-grade neuroglial, non-neuroglial, and metastasis) and a group of control brain tissue. PLS-DA revealed 9 metabolites as the most important in group differentiation: γ-aminobutyric acid, acetoacetate, alanine, creatine, glutamate/glutamine, glycine, *myo*-inositol, *N*-acetylaspartate, and choline compounds. Leave-one-out cross-validation showed that PLS-DA was efficient in group characterization. The metabolic patterns detected can be explained on the basis of previous multimodal studies of tumor metabolism and are consistent with neoplastic cell abnormalities possibly related to high turnover, resistance to apoptosis, osmotic stress and tumor tendency to use alternative energetic pathways such as glycolysis and ketogenesis.

Key words: Brain; Tumor; Magnetic resonance spectroscopy; Spectroscopy; Metabolism

Introduction

Brain cancers are estimated to be responsible for 12,920 deaths in the United States in 2009 (1). The increase in the incidence of brain tumors is partly attributable to more accurate diagnosis, especially with magnetic resonance imaging and, more recently, to the clinical application of *in vivo* proton magnetic resonance spectroscopy (^{1}H MRS). They allow early detection of the lesion and noninvasive biochemical assay of tissue in selected brain regions.

In vivo ^{1}H MRS performed at low magnetic field strengths (usually 1.5 T) is considerably limited due to resonance overlap and to line broadening. Better resolved spectra acquired *in vitro* at high resolution ^{1}H MRS are particularly useful to determine the chemical composition of tissue extracts. This procedure suffers from a degradation of the tissues

occurring before the extraction process with perchloric acid (PCA) (2). Additionally the T_2 values of the metabolites *in vitro*, in solution, are quite different from those in the tissue and the analyses rely only on water soluble metabolites missing information of the lipophilic fraction. Despite these shortcomings, the spectral features of brain tissue extract at high field strengths are similar to ^{1}H MRS *in vivo*, indicating that most biochemical information is retrieved (3).

The use of supervised pattern recognition methods such as partial least squares discriminant analysis (PLS-DA) on complex data provides a powerful tool for characterizing different classes of brain tumor extracts according to their spectral metabolic profiles (4-8). The purpose of the present study was to apply PLS-DA to analyze the high-resolution

Correspondence: A.V. Faria, 12235 Little Patuxent Pkwy, Apt. I, Columbia, MD 21044, USA. FAX: +1-443-287-6730.
E-mail: afaria1@jhmi.edu or fariaav@gmail.com

^{1}H MRS spectra of brain tumor extracts in order to refine the identification of their metabolic profile and to identify possible surrogate markers for different types of brain tumors.

Material and Methods

This study involves the use of human brain tumor biopsies. It was reviewed and approved by the Clinical Hospital Ethics Committee of the Universidade Estadual de Campinas, Brazil, where the tissue samples were obtained. The ^{1}H MRS and data analysis were performed in the Chemistry Institute, Universidade Estadual de Campinas, Brazil.

Patient group profile

High field ^{1}H MRS was applied to 43 extracts of brain tissue from 39 patients, ranging from 29 to 66 years of age, who underwent surgery or open biopsy for the treatment or diagnosis of brain tumors and from 4 patients operated for drug-resistant partial epilepsy. Except for using prednisone or manitol, the patients with brain tumors were not under any type of treatment, such as chemotherapy or radiotherapy. Tissue samples used to prepare extracts for ^{1}H MRS were taken from the same part of the tumor used for histological analysis. The main part of surgical specimens, not frozen, was processed for routine histopathology. The diagnosis was performed on 10-µm thin cryostat slices after hematoxylin-eosin staining and followed the World Health Organization (WHO) classification system. The 4 specimens from patients with partial epilepsy used as control group were taken from macroscopically normal areas, as far as possible from the focal lesion.

To simplify the statistical analyses, without affecting our objective to identify the metabolic profiles of the different tumor types, the tumor samples were divided into 4 groups: high-grade neuroglial tumors (Hg), including glioblastomas and anaplastic oligoastrocytomas; low-grade neuroglial tumors (Lg), including non-anaplastic oligoastrocytomas and grade II astrocytomas; non-neuroglial tumors (NN), including meningiomas, adenomas, schwannomas and papilloma, and metastasis from breast, lung and kidney adenocarcinomas. This grouping was based on histological and clinical characteristics of each tumor used to guide the treatment and eventually prognosis.

Sample preparation

Tissue samples (average weight = 841.25 mg) were frozen in liquid nitrogen immediately after surgical removal to minimize early changes resulting from ischemia and then stored at -80°C. Frozen tissues were weighed, minced in liquid nitrogen and then extracted with cold aqueous PCA (0.3 M, 10:1, v/w). The resulting suspensions were centrifuged (3000 g, 10 min, 0°C) and the supernatants were collected, neutralized with 1.5 M KOH (and pH adjusted to 7.2) and then lyophilized. Fifty milligrams of the lyophilized brain tumor extract was suspended in 0.6 mL D_2O containing sodium d_4-trimethylsilylpropionate (TSP; 0.625 M), used as the zero chemical shift internal standard. The solutions were sonicated, centrifuged (3000 g, 10 min, 25°C) and transferred to a 5-mm MRS tube.

MRS spectroscopy

The ^{1}H MRS spectra were acquired on a Varian INOVA-500 spectrometer (B_0 = 11.7 T), operating at 499.886 MHz for ^{1}H, using a 5-mm triple resonance (H, C, N) inverse probe with a z-gradient. Each spectrum was acquired at 25°C with 128 transients using 10,000.0 Hz spectral width, 65,536 points and 30° excitation pulse with a width of 2.2 µs. The acquisition time of each transient was 3.277 s. The intense residual water signal was suppressed using selective excitation (90° pulse) followed by a pulsed field gradient in the z-axis (wet1d). ^{1}H MRS chemical shifts and coupling constants of the most characteristic metabolites were assigned using published data (9) and standard solutions of creatine, glycerol, serine, glycine, acetate in D_2O/TSP.

Statistical analysis

For pattern recognition analysis, the spectra were digitized at intervals of 6.10 x 10^{-4} ppm over the range of 4.25-1.22 ppm, generating 4964 variables. Each individual spectrum was corrected to phase shift and point wise scaled by the sum of all intensities (normalized to unit area) to minimize the effects of necrosis in the samples. The data set was organized in the matrix format $X_{I,J}$ with dimension I = 43 rows and J = 4.964 columns where each row contained the spectrum of a brain extract.

In this study, an implementation of discriminant analysis was applied, based upon partial least squares regression, a well-established and widely used multivariate regression method (PLS-DA). In PLS, the metabolic profiles are related to a set of response variables, Y, using a series of least squares fitting steps. Collinearities in X are handled by using a projection onto a reduced-dimension subspace, for which X is given by:

$$\mathbf{X} = \sum_{r=1}^{R} \mathbf{t}_r \mathbf{p}_r^T + \mathbf{E}$$

Equation 1

where R is the number of factors in the model (or number of latent variables, LV), t and p are the scores and loading vectors for the rth factor, respectively, and the T superscript represents the matrix transpose operation. The score vectors describe the relationship between the samples in the model subspace and the loading vectors describe the importance of each variable within the model. E is the matrix of residuals, normally distributed, which could be used to determine how well each sample fitted the model. PLS scores are used for data exploration, i.e., uncovering the relationships both within and between classes of metabolic profiles. More information on this technique can be found in the literature (10,11).

PLS can be used for discriminant analysis by building

a Y matrix consisting of dummy variables used to indicate class membership. For each binary class, a column of Y is generated by assigning a value of 0 or 1 to each sample, according to its class category. For example, zero value was used for control tissue samples and one for metastasis. A schematic representation of PLS-DA is given in Figure 1. The set of responses predicted by the model was rounded to either 0 or 1, and the true and predicted class memberships were then compared to evaluate how successful the model was at classifying the given samples. Once the PLS-DA model obtained is validated it could be used to make class membership predictions for new samples, i.e., predicting Y for new measured X data.

Before building the PLS model, the data were autoscaled (each column was mean-centered and scaled by its standard deviation) to ensure that each metabolite had an equal chance to contribute to the multivariate description. The model was validated by internal leave-one-out cross-validation. Sensitivity and specificity were calculated in the largest groups through the Coomans plot. This plot contains the square distance from each sample to the reduced-dimension subspace spanned by the PLS factors, and thus, it is directly related to the matrix of residuals. Since these distances are independent and obey the normal distribution (plots not shown), the t-distribution for $I - R$ degrees of freedom gives a critical value at the 95% probability level (the critical line for each class is indicated in the plot). Sensitivity is given by the percent of brain tumors belonging to a given category and correctly identified as such and the specificity is defined as the percent of samples foreign to that category and classified as foreign.

Results

Table 1 shows the histological diagnosis of the tumor samples. The tissue from patients with epilepsy (control group) revealed heterotopia (1 patient) and glyosis (3 patients with mesial temporal sclerosis).

Nine metabolites, resonating in the spectral regions used for PLS-DA modeling, were responsible for the sample discrimination. They were selected on the basis of their contribution to the regression vector when building the model (see Figure 1) and the correlation vector containing Pearson's correlation coefficients between each variable and the class membership (each column of Y). As listed in Table 2, they are: acetoacetate (Ac), alanine (Ala), creatine (Cr), choline compounds [composed of free choline (Cho), glycerophosphocholine (GPC) and phosphocholine (PC)], γ-aminobutyric acid (GABA), glycine (Gly), glutamine and glutamate (Gln/Glu), *myo*-inositol (m-Ins), and *N*-acetyl aspartate (NAA).

Distinction between Hg and Lg tumors

Selected variables from ^{1}H MRS spectra of Hg and Lg tumors are highlighted in Figure 2 (top left). These re-

gions, which correspond to the metabolites of interest, are expanded to show their importance to discriminate the two types of tumors. Hg tumors (black profiles) showed a relative abundance of Gly, Ala, and Gln/Glu. m-Ins was decreased in Hg compared to Lg tumors (green profiles).

The PLS model was built on the selected variables for 18 samples (Table 2). The number of factors in the model, LV = 1, determined by cross-validation, and the correlation coefficient, r = 0.86, was sufficient to discriminate both classes of tumors. Figure 2B shows the score plot for factor 1 (f1) versus factor 2 (f2). This plot shows how
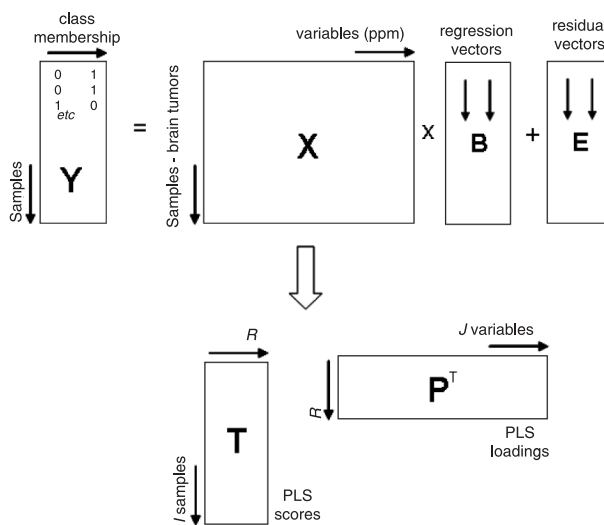
Figure 1. Schematic representation of PLS-DA. The matrix, which defines the class membership for each sample, Y, is regressed against the matrix of spectral profiles, X.

Table 1. Classification of brain tumor samples used in the present study according to the WHO.

Groups	Number of samples
High-grade neuroglial tumors (Hg)	
Grade IV astrocytomas	10
Anaplastic oligoastrocytomas	3
Low-grade neuroglial tumors (Lg)	
Grade II astrocytomas	3
Non-anaplastic oligoastrocytomas	2
Non-neuroglial tumors (NN)	
Meningiomas	10
Schwannomas	2
Adenomas	3
Papilloma	1
Metastasis	5
Controls	4

the samples are clustered in the subspace defined by the first two LVs of the PLS model, describing 43.2% of the original information.

Distinction between NN and neuroglial tumors

The same procedure described previously was applied to both data sets: NN and Hg; NN and Lg tumors. NN tumors (blue profiles) were characterized for having lower levels of Cr and NAA when compared to both Lg (Figure 3, green profiles) and Hg tumors (Figure 4, black profiles). NN also showed a higher relative abundance of Ala and Gly when compared with Lg tumors and Ac when compared with Hg tumors. m-Ins and Gln/Glu levels were relatively increased in Lg and Hg tumors, respectively. From the PLS score plot in Figure 3 (where two factors account for 50.9% of total variance) one can see that factor one (f1) is enough to discriminate NN from neuroglial tumors. That does not happen for NN and Hg tumors in Figure 4, where 2 factors were determined by cross-validation. From the PLS score plot (Figure 4B) it is clear that one factor was not enough to discriminate both types of tumors.

In order to increase the reliability of the PLS-DA model, the specificity and sensitivity were calculated for the largest groups. Figure 5 shows the Comman plot for the comparison between Hg vs NN tumors, the two largest groups. According to this analysis, samples in the second and fourth quadrants belong to Hg and NN tumor categories, respectively. Those in the third quadrant were classified as belonging to both classes. Both models have a sensitivity of 100%, which means that are able to correctly recognize all the samples from their group. On the other hand, Hg and NN classes have a specificity of 50 and 37.5%, respectively. This means that Hg class is capable of identifying 50% of

samples from NN tumors while NN class is able to recognize 62.5% of Hg tumors.

Distinction between metastasis and Hg tumors and metastasis and NN tumors

Metastasis (red profiles) had lower levels of m-Ins and Gln/Glu when compared with both Hg (Figure 6, black profiles) and NN tumors (Figure 7, blue profiles) and a particular distribution of Cho compounds with higher PC peak. NAA and Cr were important only in differentiating Hg tumors, depicting lower contents in metastasis. Using two LVs, a reasonable separation of respective classes was obtained (Figures 6B and 7B) with high correlation coefficients (r = 0.82 and 0.84 for data in Figures 6 and 7, respectively). During the cross-validation, two metastasis samples were misclassified (circled in Figure 6). Although these samples were found to fit the model quite poorly, they were retained in order to maintain a minimum realistic level of sample variability.

Distinction between metastasis and Lg tumors

Despite the fact that these were small groups, some tendencies could be observed upon inspection of the expanded regions corresponding to the metabolites highlighted in the full spectra (Figure 8, upper left): metastasis had higher levels of Ala and Gly and lower levels of m-Ins, Cr and NAA. Again, as confirmed by the score plot, one LV produced a reasonable separation of respective classes (Figure 8B) with r = 0.88.

Distinction between controls and tumors (except Lg tumors)

Tumors (light green profiles, in Figure 9) had great amounts of Ala and PC and reduced Cr, m-Ins, NAA, and

Table 2. Spectral regions used for building the PLS-DA regression models.

| Spectral region (ppm)	Metabolite: shift in ppm (multiplicity, coupling constants J in Hz)	Variable used in:
4.085-4.053	m-Ins: 4.07 (t, 2.9)	LgxHg, LgxNN, LgxM
3.94-3.927	Cr: 3.94 (s)	HgxNN, HgxM, LgxNN, LgxM, NNxM
3.648-3.479	m-Ins: 3.63 (t, 9.8), 3.55 (dd, 10.0 and 2.9), Gly: 3.57 (s)	LgxHg, LgxNN, HgxM, MxNN, MxLg, TxC
3.311-3.261	m-Ins: 3.29 (t, 9.3)	HgxLg, LgxM
3.252-3.201	Cho: 3.21 (s), PC: 3.23 (s), GPC: 3.24 (s)	MxHg, MxLg, MxNN, CxT
3.051-3.034	Cr: 3.04 (s)	HgxNN, HgxM, LgxNN, LgxM, CxT
2.495-2.430; 2.17-2.112	Gln/Glu: (m)	HgxLg, HgxM,
2.322-2.283	GABA: 2.30 (t, 7.3)	CxT
2.244-2.225	Ac: 2.24 (s)	HgxNN
2.034-2.015	NAA: 2.02 (s)	HgxNN, HgxM, LgxNN, LgxM, CxT
1.499-1.468	Ala: 1.49 (d, 7.2)	LgxHg, LgxM, LgxNN, CxT

m-Ins = *myo*-inositol; Cr = creatine; Gly = glycine; Cho = choline; PC = phosphocholine; GPC = glycerophosphocholine; Gln/Glu = glutamine and glutamate; GABA = γ-aminobutyric acid; Ac = acetoacetate; NAA = *N*-acetyl aspartate; Ala = alanine. Multiplicity: s = singlet; d = doublet; dd = double doublet; t = triplet; q = quartet; m = other multiplet. Lg = low-grade neuroglial tumors; Hg = high-grade neuroglial tumors; NN = non-neuroglial tumors; M = metastasis; T = tumor; C = control.
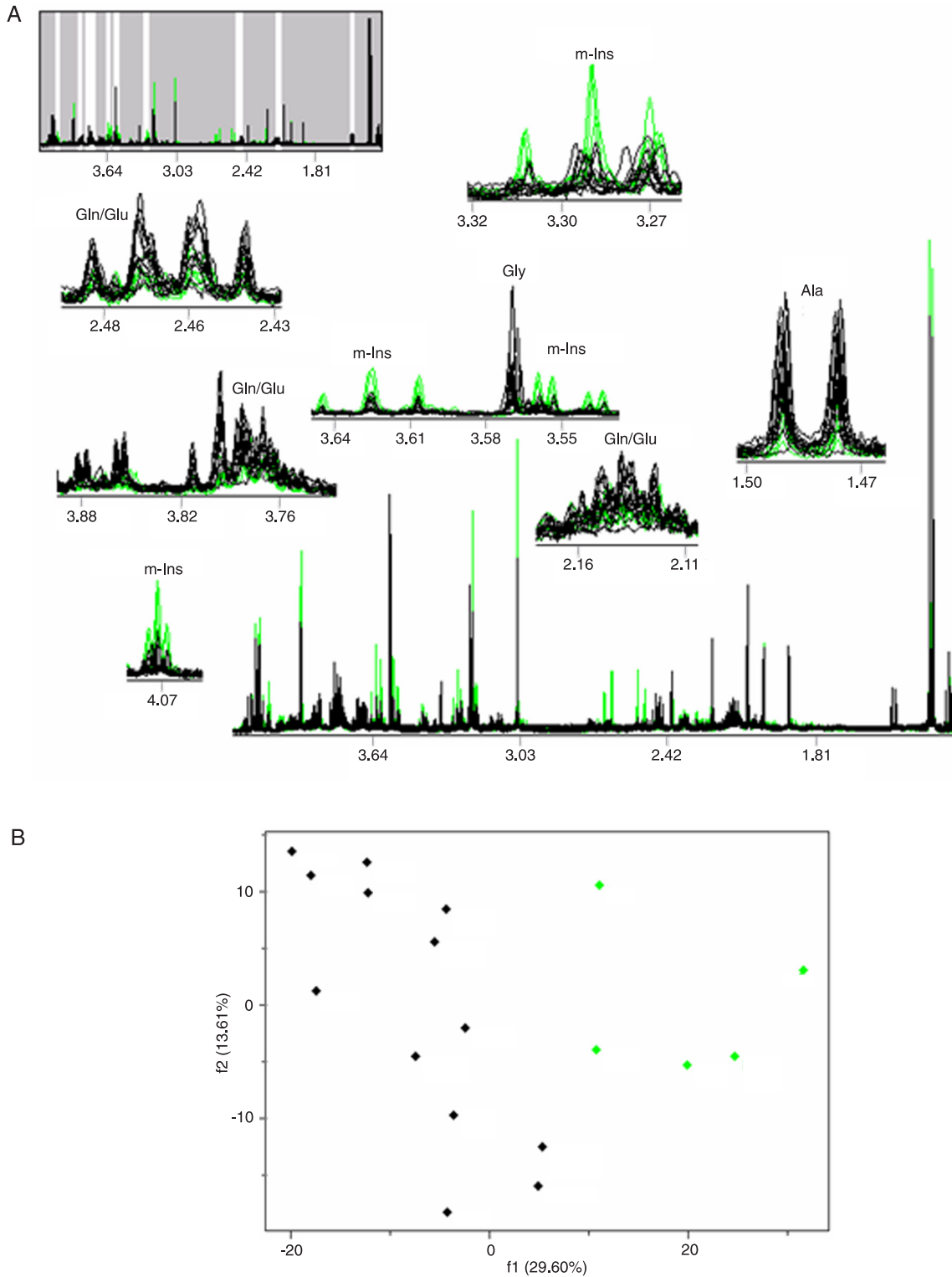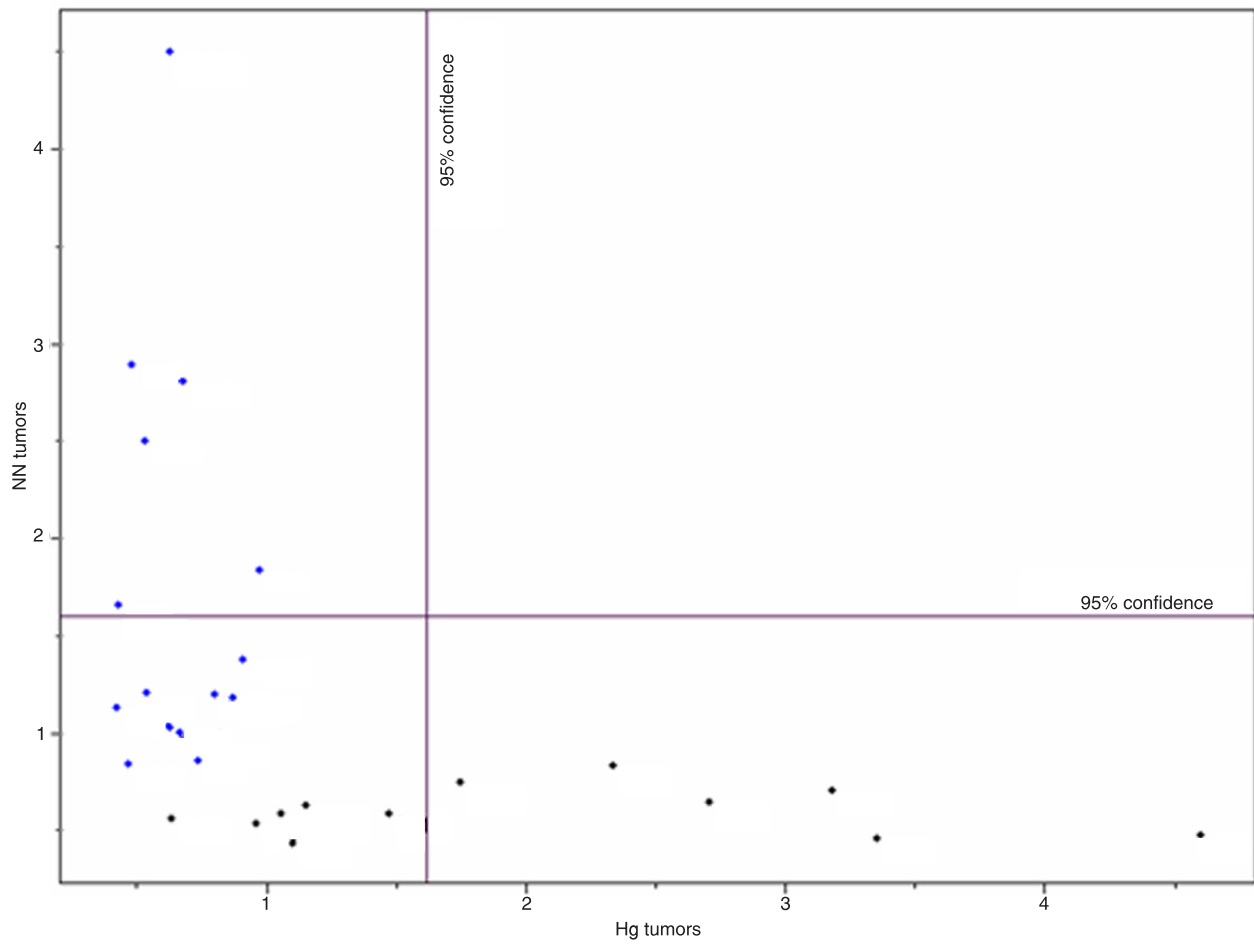
Figure 2. *A*, ¹H MRS spectral profiles. Full spectra superimposed with the metabolites of interest highlighted (superior, left) and the expanded regions of interest to emphasize the differences between high-grade neuroglial tumors (black) and low-grade neuroglial tumors (green). *B*, Score plot of factor 1 (f1) *vs* factor 2 (f2) from PLS model (r = 0.86) built with 1 latent variable. Percentages in x- and y-axes refer to the amount of variance explained by the corresponding factor. For metabolite abbreviations, see legend to Table 2.
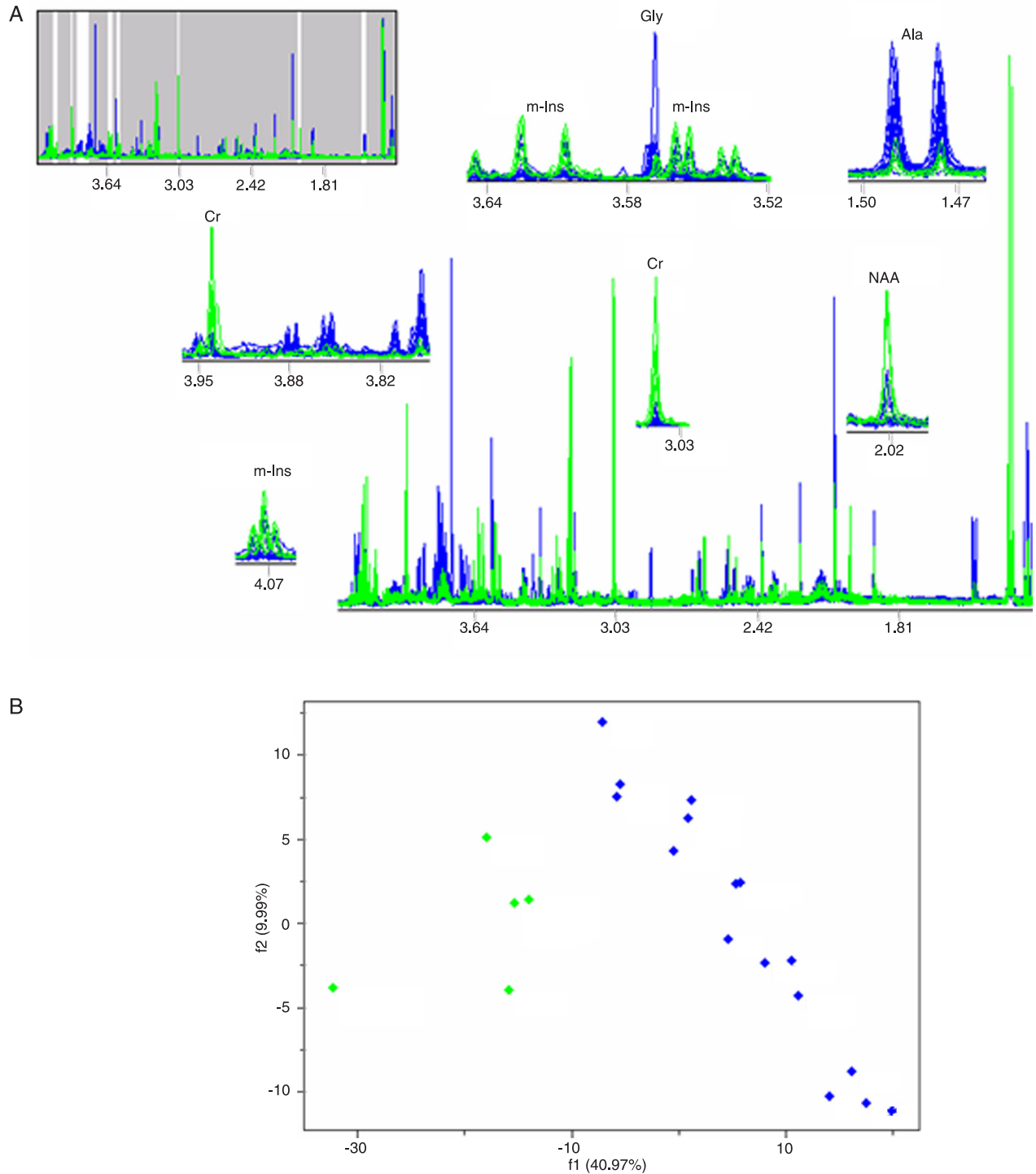
Figure 3. *A*, ^{1}H MRS spectral profiles: low-grade neuroglial tumors (green) and non-neuroglial tumors (blue). The expanded regions of interest emphasize the differences between the referred groups. *B*, Score plot of factor 1 (f1) *vs* factor 2 (f2) from PLS model (r = 0.80) built with 1 latent variable. Percentages in x- and y-axes refer to the amount of variance explained by the corresponding factor. For metabolite abbreviations, see legend to Table 2.
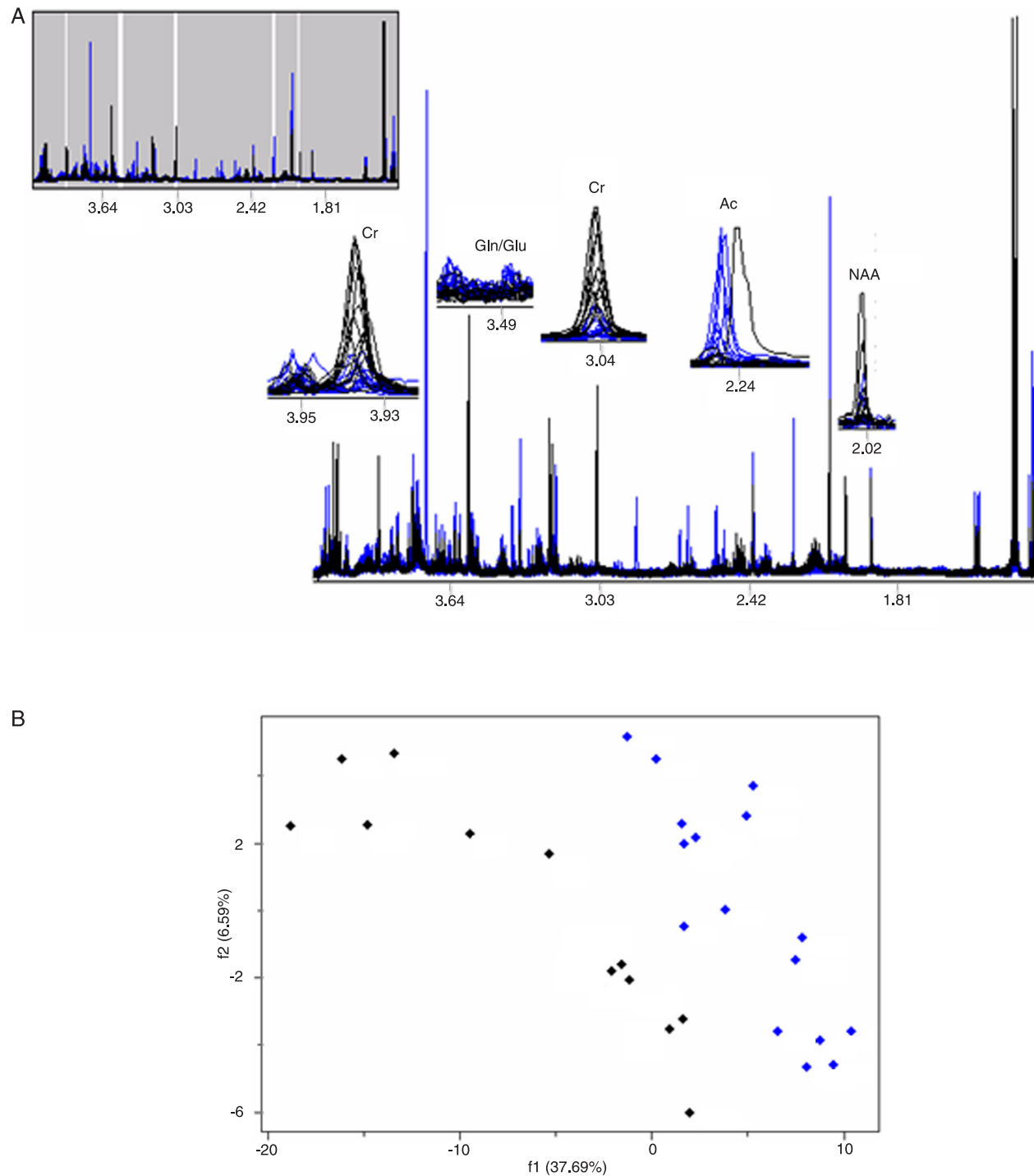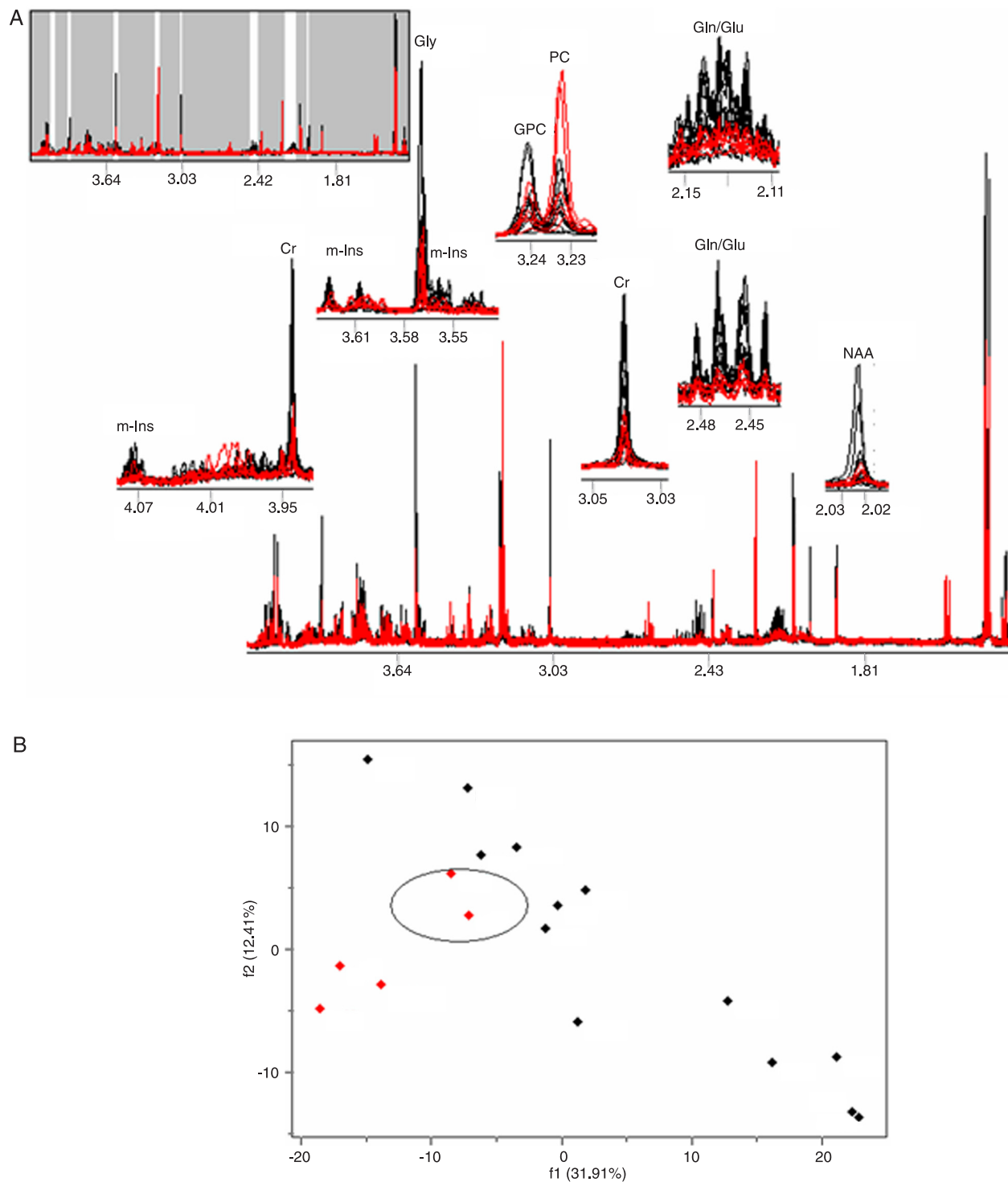
Figure 4. *A*, ^{1}H MRS spectral profiles: high-grade neuroglial tumors (black) and non-neuroglial tumors (blue). *B*, Score plot of factor 1 (f1) *vs* factor 2 (f2) from PLS model (r = 0.88) built with 2 latent variables. Percentages in x- and y-axes refer to the amount of variance explained by the corresponding factor. For metabolite abbreviations, see legend to Table 2.

Figure 5. Coomans plot for the square distances of non-neuroglial (NN, blue) and high-grade neuroglial (Hg, black) tumors to their respective subspaces defined by the PLS factors.

Figure 6. *A*, ¹H MRS spectral profiles: high-grade neuroglial tumors (black) and metastasis (red). *B*, Score plot of factor 1 (f1) *vs* factor 2 (f2) from PLS model (r = 0.82) built with 2 latent variables. The circle marks the two samples that were misclassified in the "leave-one-out" cross-validation. For metabolite abbreviations, see legend to Table 2.
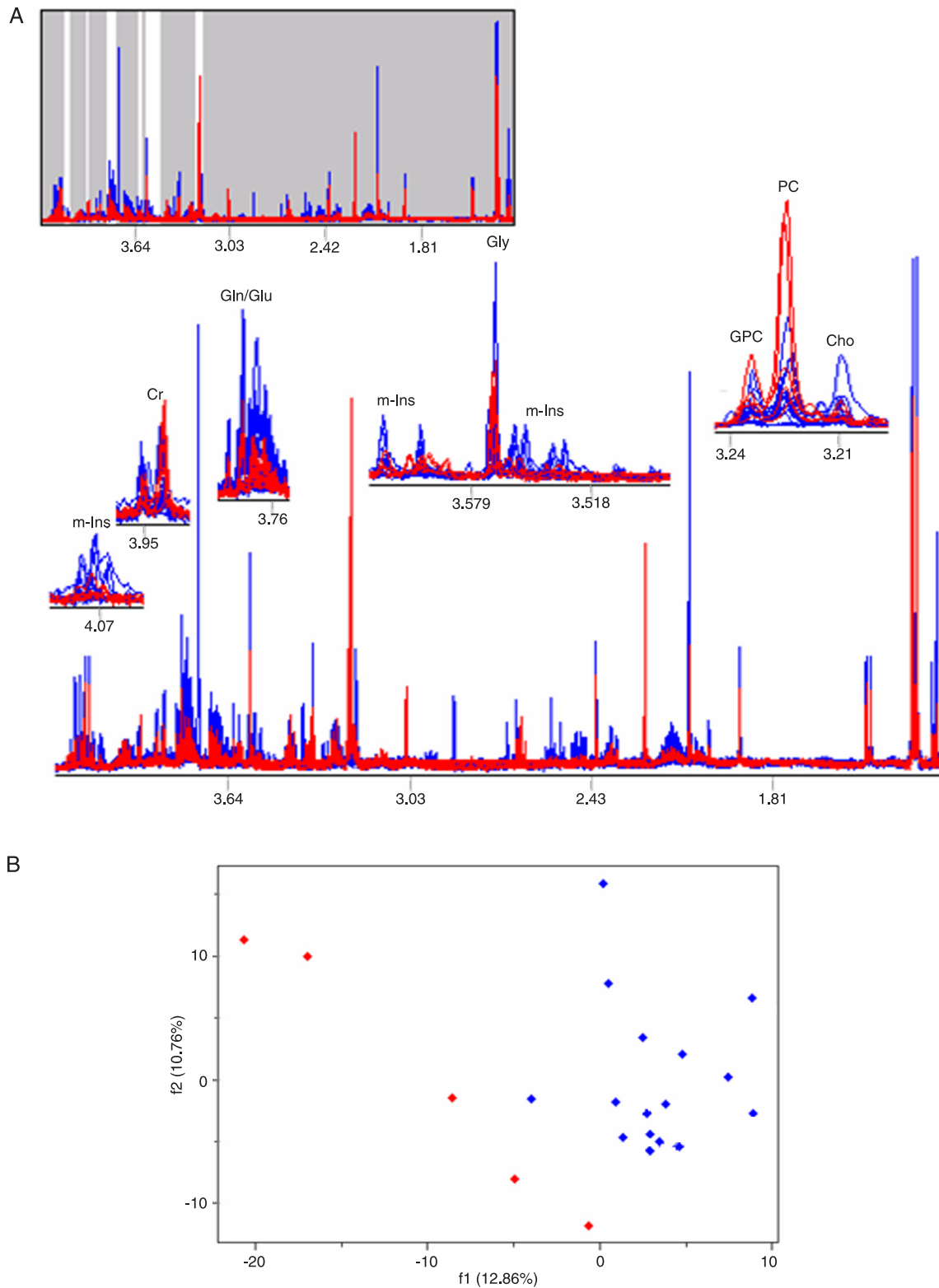
Figure 7. *A*, ^{1}H MRS spectral profiles: metastasis (red) and non-neuroglial tumors (blue). *B*, Score plot of factor 1 (f1) *vs* factor 2 (f2) from PLS model (r = 0.84) built with 2 latent variables. For metabolite abbreviations, see legend to Table 2.
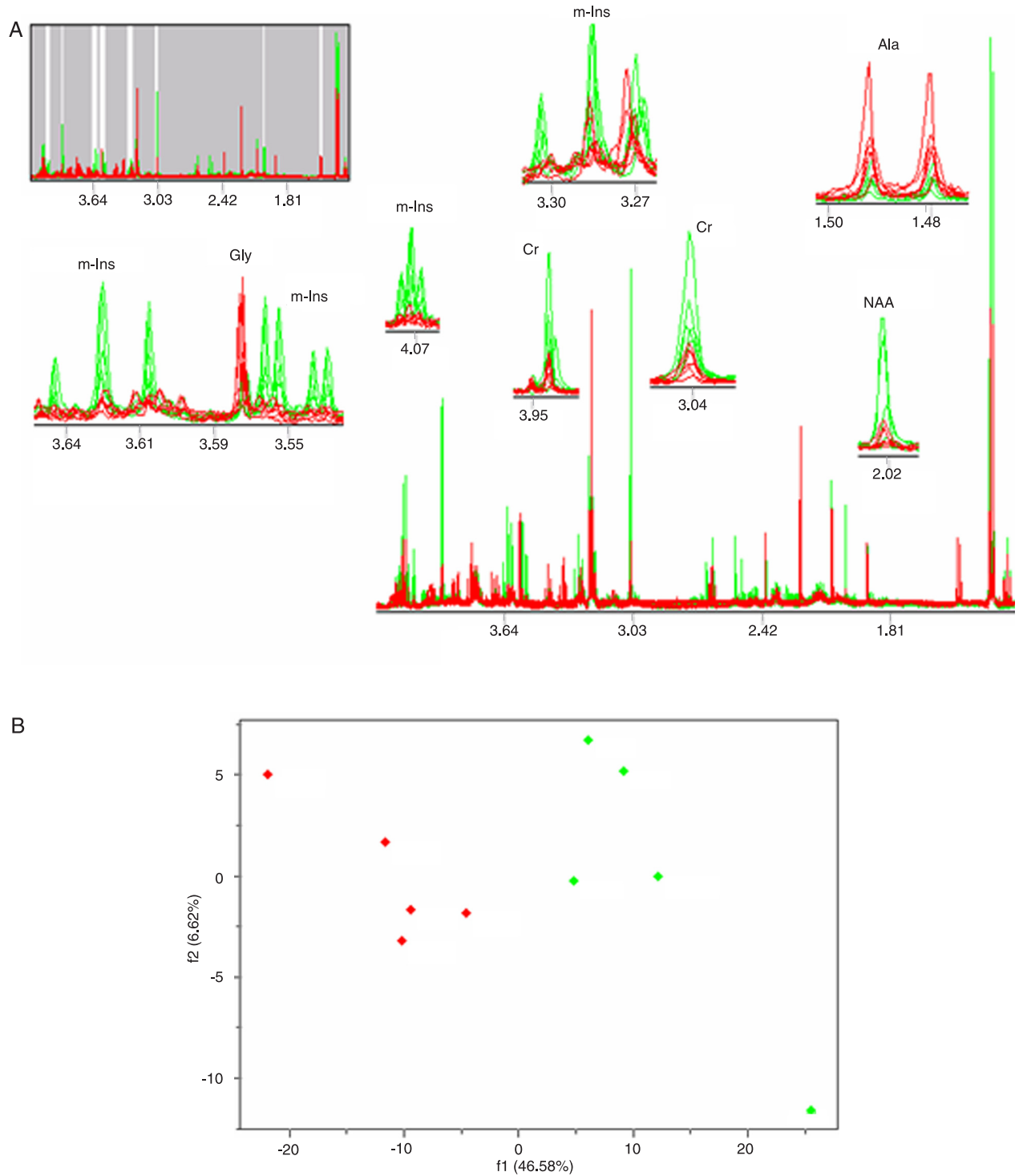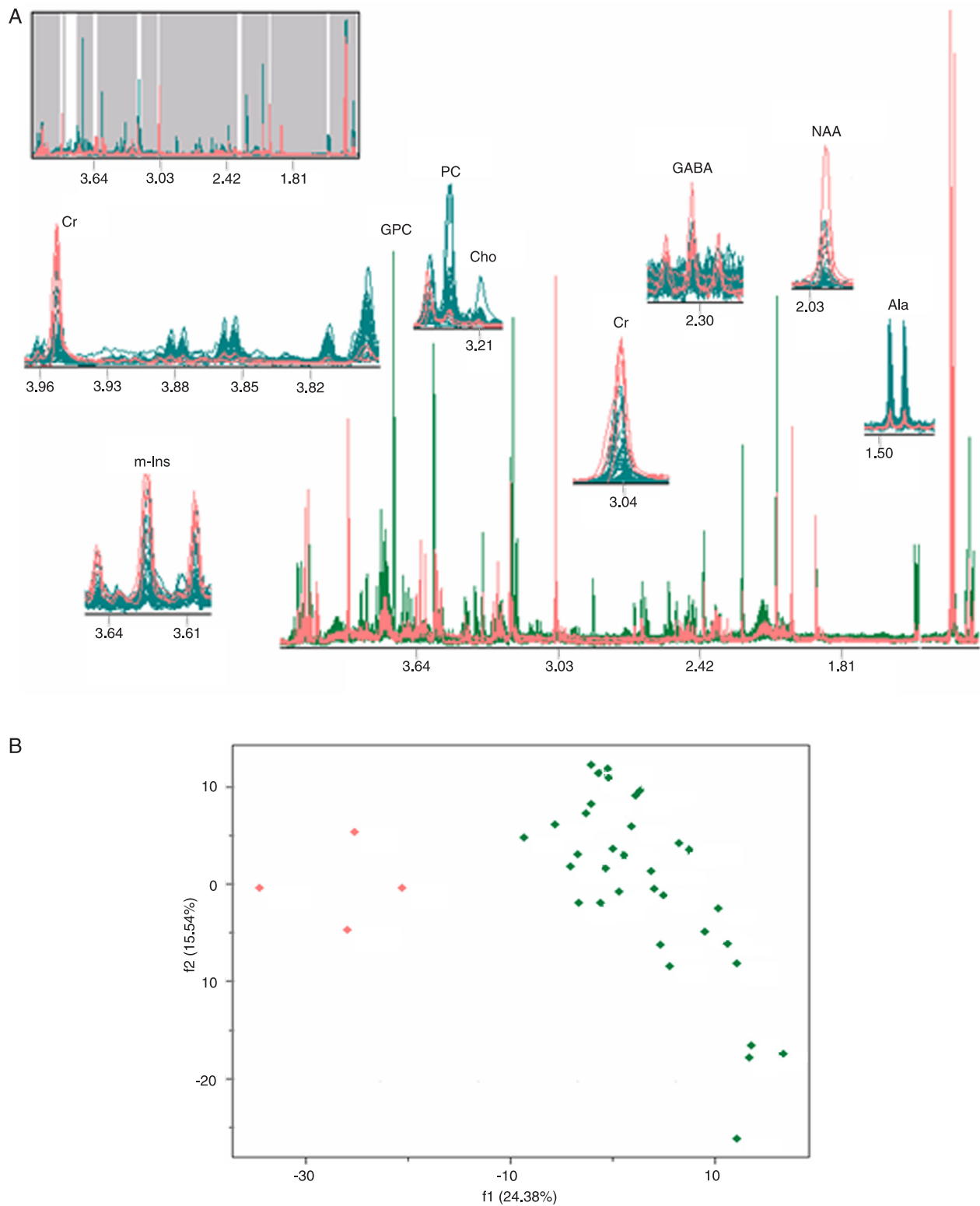
Figure 8. *A*, ¹H MRS spectral profiles: low-grade neuroglial tumors (green) and metastasis (red). *B*, Score plot of factor 1 (f1) *vs* factor 2 (f2) from PLS model (r = 0.88) built with 1 latent variable. For metabolite abbreviations, see legend to Table 2.

Figure 9. *A,* ^{1}H MRS spectral profiles: tumors (light green), except low-grade neuroglial ones, and controls (salmon). *B,* Score plot of factor 1 (f1) *vs* factor 2 (f2) from PLS model (r = 0.91) built with 2 latent variables. For metabolite abbreviations, see legend to Table 2.

Table 3. Summary of PLS-DA classification results obtained from leave-one-out cross-validation.

Sample type	Control (C)	Low-grade neuroglial tumors (Lg)	High-grade neuroglial tumors (Hg)	Non-neuroglial tumors (NN)	Metastases (M)	Misses
No. of samples	4	5	13	16	5	
Lg/NN		5		16		0
Lg/M		5			5	0
Hg/M			15		3	2
Hg/Lg		5	13			0
NN/M				16	5	0
Tumors*/C	4		13	16	5	0
Hg/NN			13	16		0

*Except low-grade neuroglial tumors.

GABA as compared with the control group (salmon profiles). This was the only case where the separation between the two clusters could be observed in f1 although the number suggested by cross-validation in the PLS model was LV = 2. One extra factor is required in order to better describe the variability in the sample mode or to compensate for possible non-linearity in the spectral mode.

It was not possible to build a good model to differentiate controls from Lg tumors by PLS-DA, probably due the reduced number of samples and tissue similarities.

Finally, the results from 'leave-one-out' analysis, summarized in Table 3, show that from all PLS-DA analyses only two incorrect classifications occurred when 2 metastasis samples were classified as Hg tumor.

Discussion

We used high field ^{1}H MRS in order to improve the identification of the biochemical profiles in brain tumor extracts. Application of PLS-DA allowed the identification of different metabolites and their correlation with distinct tumor types. Recently, multiple studies, such as the multicenter "eTUMOR" and "INTERPRET", have shown similar results from the analysis of MRS with multivariate models (4-8). The advantage of these methods for data analyses is that they can simultaneously handle a large range of metabolites providing a powerful tool for profile discrimination thus reducing the large number of spectral variables to a few key metabolites.

The predicted classes by "leave-one-out" cross-validation indicates PLS-DA as an excellent classification method for ^{1}H MRS spectral data. In addition to the small number of errors, the model did not misclassify any control or Lg tumor samples and the 2 incorrect classifications occurred in groups that, despite histological difference, have similar aggressiveness (metastasis and Hg tumor, see Table 3).

Our results demonstrated higher amounts of Gly in aggressive tumors (Hg and metastasis) compared with Lg (Figures 2 and 8) and lower levels of m-Ins in all tumor groups with the exception of Lg group (Figure 9) compared to control samples, a characteristic that was more evident in the aggressive ones, Hg and metastasis (Figures 2, 6, 7, and 8). In addition to changes related to tumor metabolism, such as anti-apoptotic activity (12), protection against nutrient starvation and hyperosmolarity, regulation of mitochondrial permeability transition (13), and participation in tricarboxylic acid cycle, Gly levels decrease less than those of other metabolites in the areas of tissue necrosis in aggressive tumors (14). On the other hand, m-Ins is present in glial cell cultures and its levels increase according to the number of normal glial cells (15). Therefore, m-Ins reduction or absence in Hg, NN and metastasis groups indirectly indicates the absence or reduction of normal glial cells. In this study, the increase of Gly and the decrease of m-Ins were a general tendency in aggressive tumors, as recently described in *in vivo* and *in vitro* studies (16,17). However, at low magnetic fields with TEs of 135-270 ms, *in vivo* studies have shown a marked signal overlapping of m-Ins with Gly methylene at δ 3.56 ppm and these two metabolites are usually evaluated together, limiting their diagnostic value. Guided by these findings, the observation of the signal decay from short to long TE at lower fields, where m-Ins decays faster, and the use of TEs as low as 30 ms at 7 T *in vivo,* which are able to differentiate these peaks (18), could be useful for the clinical investigation of aggressive tumors.

We noticed higher levels of Gln/Glu in Hg neuroglial tumors (Figures 2 and 6), which also occurred in previous *in vivo* and *in vitro* studies (19). It is interesting to note that, in controls, Gln/Glu levels were slightly higher than in Lg tumors though not enough to differentiate them. This was believed to be due to the fact that the control samples were provided with areas of epileptiform activity (20). As m-Ins, Gln is primarily of astrocytic origin, despite being also present in NN cells (21). Our NN tumor samples also presented a discrete increase of Gln/Glu with respect to the metastasis (Figure 7) and no differences in relation to

the Lg ones (Figure 3). Therefore, Gln/Glu could be related to both histological type and tumor metabolism, which deserves further investigation.

Ala was increased in all tumor groups compared to controls (Figure 9). This is in agreement with other studies that showed that Ala concentration is much higher in brain tumor extracts (22). Increased Ala has been observed *in vivo* in meningiomas (23) and less frequently in other tumors. In NN tumors (Figure 3) the Ala increase is attributed not only to typical tumor pathways but also to the composition of original tumor cells since Ala concentration is three times higher in meningeal cells than in neurons (24). In addition, aggressive tumors such as metastasis and Hg tumors, usually have higher amounts of lipids that can cause an overlap with Ala peak *in vivo*, potentially preventing its precise measurement (21). Another difficulty for this measurement is that Ala level in normal brain is below the *in vivo* MRS detection threshold and only major variations could be detected. The same reasoning might be applied to the Ac, a product of amino acids (as Ala) degradation, that had increased levels in NN tumors, when compared with Hg tumors (Figure 4).

Cr levels were reduced in tumors (Figure 9), particularly in Hg ones (Figures 4 and 6) but also in NN and metastasis when compared with Lg tumors (Figures 3 and 8, respectively). In tumors, alterations in oxidative phosphorylation linked to rapid cell proliferation are usually related to low Cr levels since Cr is a secure marker of endogenous metabolism and energetic state of brain cells (25).

Similar alterations occurred with NAA levels. We observed relative decreased levels in tumors (Figure 9), particularly in Hg ones (Figure 4) but also in NN and metastasis when compared with Lg tumors (Figures 3 and 8, respectively). This decrease probably indicates absence of mature neurons (26,27) in Hg tumors and, obviously, in NN tumors and metastasis. However, contrary to the *in vivo* studies, NAA was not important in differentiating Hg from Lg tumors (Figure 2) and Lg tumors from controls. This could be explained in part by the great variation in NAA concentration in Hg samples and by the fact that our control samples are from epileptic patients, a condition related with NAA decrease (28).

GABA was selected as an important metabolite in tumor and control tissue differentiation (Figure 9). It was detected only in control and Lg tumor extracts. GABA alterations have been reported before in epilepsy MRS studies (26) but in tumors its importance has been poorly discussed. Likewise NAA, GABA is related with neuronal (but also glial) metabolism, once it is the mainly inhibitory neurotransmitter, synthesized from glutamate in neurons. One hypothesis is that the absence of mature and/or well-differentiated neurons and glial cells in these tumors could be related with GABA decrease, but since there are no data to support this theory in the present study, it is purely speculative.

An additional unusual observation concerns to choline peak, composed by GPC, PC and Cho. We noticed a particular distribution of Cho compounds in tumors. They had a tendency in increasing PC (Figure 9), particularly in metastasis (Figures 6, 7, and 8). This is a novel observation in MRS of metastasis. Increased levels of Cho, a cellular membrane phospholipid, are related to the high cellular turnover in tumors. However, Cho is very sensitive to the tumor necrosis. Consequently, due to the high heterogeneity of neuroglial tumors, the significance of *in vivo* ^{1}H MRS total Cho level is actually controversial (29).

Nevertheless, the differences in the Cho-containing compounds could be an important tumor marker. Elevated [PC] / [GPC] values were reported recently in a number of malignant tumor cells, derived from mesenchymal (meningioma), glial (glioblastoma) (30) and neuronal (neuroblastoma) tissues (31) while in "normal" peripheral tumor tissue there is a large predominance of GPC (32). Previous studies detected overexpression of choline kinase alpha (ChoK), an enzyme involved in the synthesis of phosphatidylcholine, in a variety of human cancers (33). Therefore, our findings encourage the use of *in vivo* techniques that could efficiently differentiate PC and GPC (17) in the investigation of glial tumors and metastasis.

Classic biochemical studies have demonstrated that the vast majority of human and animal tumors have a high glycolysis rate, even under aerobic conditions (Warburg effect), an observation that has repeatedly been confirmed (34). Since Lac is the one of the main glycolysis product, this metabolite is expected to be an important tumor marker (35-38). However, in our study, Lac was not an important peak in PLS-DA. This was assigned to its fast and variable accumulation during and after the surgical procedure (39) leading to an irregular and unrestricted elevation of its levels in the samples.

It was not possible to build a PLS model capable to differentiate Lg tumors and controls. In addition to the small number of samples in both groups we recognize that our control samples were extracted from epileptogenic areas that could present an abnormal metabolic profile, including alterations in NAA, GABA, Cho, and Cr (40). We assigned this impossibility also to metabolic similarity between these groups (Lg tumors are biologically closer to controls than any other tumor group) and the fact that Lg tumors infiltrate normal brain. Therefore, the Lg samples analyzed might contain variable proportions of "normal tissue".

One limitation of the present study is the number of samples, particularly in groups such as metastasis and Lg tumors. In these small groups, the specificity and sensitivity of the classification proposed here is smaller than that found in larger groups (Figure 5). Although we performed an "internal validation" using leave-one-out analysis and the models we obtained are in agreement with the previous studies discussed above, we are aware that the increase of the number of samples and an "external validation" us-

ing a second group would be necessary to validate and optimize our models. However, the current data are useful as a demonstration of the utility of this technique for biochemical classification of brain tumors. Nevertheless, this is the first step toward the improvement of our knowledge about the pathways that regulate brain tumor survival and, hopefully, at long term, this technique would represent an important tool for the diagnosis and for the design of specific therapy strategies.

References

1. American Cancer Society. http://www.cancer.org/.

2. Perry TL, Hansen S, Gandham SS. Postmortem changes of amino compounds in human and rat brain. *J Neurochem* 1981; 36: 406-410.

3. Martinez-Bisbal MC, Marti-Bonmati L, Piquer J, Revert A, Ferrer P, Llacer JL, et al. [1]H and ^{13}C HR-MAS spectroscopy of intact biopsy samples *ex vivo* and *in vivo* ^{1}H MRS study of human high grade gliomas. *NMR Biomed* 2004; 17: 191-205.

4. Garcia-Gomez JM, Luts J, Julia-Sape M, Krooshof P, Tortajada S, Robledo JV, et al. Multiproject-multicenter evaluation of automatic brain tumor classification by magnetic resonance spectroscopy. *MAGMA* 2009; 22: 5-18.

5. Tate AR, Underwood J, Acosta DM, Julia-Sape M, Majos C, Moreno-Torres A, et al. Development of a decision support system for diagnosis and grading of brain tumours using *in vivo* magnetic resonance single voxel spectra. *NMR Biomed* 2006; 19: 411-434.

6. Wright AJ, Arus C, Wijnen JP, Moreno-Torres A, Griffiths JR, Celda B, et al. Automated quality control protocol for MR spectra of brain tumors. *Magn Reson Med* 2008; 59: 1274-1281.

7. Julia-Sape M, Acosta D, Mier M, Arus C, Watson D. A multi-centre, web-accessible and quality control-checked database of *in vivo* MR spectra of brain tumour patients. *MAGMA* 2006; 19: 22-33.

8. Solivera J, Cerdan S, Pascual JM, Barrios L, Roda JM. Assessment of ^{31}P-NMR analysis of phospholipid profiles for potential differential diagnosis of human cerebral tumors. *NMR Biomed* 2009; 22: 663-674.

9. Govindaraju V, Young K, Maudsley AA. Proton NMR chemical shifts and coupling constants for brain metabolites. *NMR Biomed* 2000; 13: 129-153.

10. Geladi P, Kowalski BR. Partial least squares regression: A tutorial. *Anal Chim Acta* 1986; 185: 1-17.

11. Ferreira MMC, Antunes AM, Melo MS, Volpe PLO. [Chemometrics I: multivariate calibration, a tutorial. *Quím Nova* 1999; 22: 724-731.

12. Sharipo A, Imreh M, Leonchiks A, Imreh S, Masucci MG. A minimal glycine-alanine repeat prevents the interaction of ubiquitinated I kappaB alpha with the proteasome: a new mechanism for selective inhibition of proteolysis. *Nat Med* 1998; 4: 939-944.

13. Lemasters JJ, Qian T, He L, Kim JS, Elmore SP, Cascio WE, et al. Role of mitochondrial inner membrane permeabilization in necrotic cell death, apoptosis, and autophagy.

Antioxid Redox Signal 2002; 4: 769-781.

14. Lehnhardt FG, Rohn G, Ernestus RI, Grune M, Hoehn M. [1]H- and ^{31}P-MR spectroscopy of primary and recurrent human brain tumors *in vitro*: malignancy-characteristic profiles of water soluble and lipophilic spectral components. *NMR Biomed* 2001; 14: 307-317.

15. Brand A, Richter-Landsberg C, Leibfritz D. Multinuclear NMR studies on the energy metabolism of glial and neuronal cells. *Dev Neurosci* 1993; 15: 289-298.

16. Majos C, Aguilera C, Alonso J, Julia-Sape M, Castaner S, Sanchez JJ, et al. Proton MR spectroscopy improves discrimination between tumor and pseudotumoral lesion in solid brain masses. *AJNR Am J Neuroradiol* 2009; 30: 544-551.

17. Loening NM, Chamberlin AM, Zepeda AG, Gonzalez RG, Cheng LL. Quantification of phosphocholine and glycerophosphocholine with ^{31}P edited ^{1}H NMR spectroscopy. *NMR Biomed* 2005; 18: 413-420.

18. Gambarota G, Mekle R, Xin L, Hergt M, van der Zwaag W, Krueger G, et al. *In vivo* measurement of glycine with short echo-time ^{1}H MRS in human brain at 7 T. *MAGMA* 2009; 22: 1-4.

19. Lehnhardt FG, Bock C, Rohn G, Ernestus RI, Hoehn M. Metabolic differences between primary and recurrent human brain tumors: a ^{1}H NMR spectroscopic investigation. *NMR Biomed* 2005; 18: 371-382.

20. Otsuki T, Nakama H, Kanamatsu T, Tsukada Y. Glutamate metabolism in epilepsy: ^{13}C-magnetic resonance spectroscopy observation in the human brain. *Neuroreport* 2005; 16: 2057-2060.

21. Urenjak J, Williams SR, Gadian DG, Noble M. Proton nuclear magnetic resonance spectroscopy unambiguously identifies different neural cell types. *J Neurosci* 1993; 13: 981-989.

22. Peeling J, Sutherland G. High-resolution ^{1}H NMR spectroscopy studies of extracts of human cerebral neoplasms. *Magn Reson Med* 1992; 24: 123-136.

23. Poptani H, Gupta RK, Jain VK, Roy R, Pandey R. Cystic intracranial mass lesions: possible role of *in vivo* MR spectroscopy in its differential diagnosis. *Magn Reson Imaging* 1995; 13: 1019-1029.

24. Demir MK, Iplikcioglu AC, Dincer A, Arslan M, Sav A. Single voxel proton MR spectroscopy findings of typical and atypical intracranial meningiomas. *Eur J Radiol* 2006; 60: 48-55.

25. Rothman DL, Behar KL, Hetherington HP, Shulman RG. Homonuclear ^{1}H double-resonance difference spectroscopy

of the rat brain *in vivo*. *Proc Natl Acad Sci U S A* 1984; 81: 6330-6334.

26. Bernasconi A, Tasch E, Cendes F, Li LM, Arnold DL. Proton magnetic resonance spectroscopic imaging suggests progressive neuronal damage in human temporal lobe epilepsy. *Prog Brain Res* 2002; 135: 297-304.

27. Petroff OA, Errante LD, Kim JH, Spencer DD. N-acetyl-aspartate, total creatine, and myo-inositol in the epileptogenic human hippocampus. *Neurology* 2003; 60: 1646-1651.

28. Gill M, Miller SL, Evans D, Scatliff JH, Meyerand ME, Powers SK, et al. Magnetic resonance imaging and spectroscopy of small ring-enhancing lesions using a rat glioma model. *Invest Radiol* 1994; 29: 301-306.

29. Simister RJ, McLean MA, Barker GJ, Duncan JS. Proton magnetic resonance spectroscopy of malformations of cortical development causing epilepsy. *Epilepsy Res* 2007; 74: 107-115.

30. Sabatier J, Gilard V, Malet-Martino M, Ranjeva JP, Terral C, Breil S, et al. Characterization of choline compounds with *in vitro* ^{1}H magnetic resonance spectroscopy for the discrimination of primary brain tumors. *Invest Radiol* 1999; 34: 230-235.

31. Miller BL, Chang L, Booth R, Ernst T, Cornford M, Nikas D, et al. *In vivo* ^{1}H MRS choline: correlation with *in vitro* chemistry/histology. *Life Sci* 1996; 58: 1929-1935.

32. Usenius JP, Kauppinen RA, Vainio PA, Hernesniemi JA, Vapalahti MP, Paljarvi LA, et al. Quantitative metabolite patterns of human brain tumors: detection by ^{1}H NMR spectroscopy *in vivo* and *in vitro*. *J Comput Assist Tomogr* 1994; 18: 705-713.

33. Gallego-Ortega D, Ramirez De MA, Gutierrez R, Ramos MA, Sarmentero J, Cejas P, et al. Generation and characterization of monoclonal antibodies against choline kinase alpha and their potential use as diagnostic tools in cancer. *Int J Oncol* 2006; 29: 335-340.

34. Ravi R, Mookerjee B, Bhujwalla ZM, Sutter CH, Artemov D, Zeng Q, et al. Regulation of tumor angiogenesis by p53-induced degradation of hypoxia-inducible factor 1 alpha. *Genes Dev* 2000; 14: 34-44.

35. Gracey AY, Troll JV, Somero GN. Hypoxia-induced gene expression profiling in the euryoxic fish *Gillichthys mirabilis*. *Proc Natl Acad Sci U S A* 2001; 98: 1993-1998.

36. Huang LE, Bunn HF. Hypoxia-inducible factor and its biomedical relevance. *J Biol Chem* 2003; 278: 19575-19578.

37. Jogi A, Ora I, Nilsson H, Lindeheim A, Makino Y, Poellinger L, et al. Hypoxia alters gene expression in human neuroblastoma cells toward an immature and neural crest-like phenotype. *Proc Natl Acad Sci U S A* 2002; 99: 7021-7026.

38. Seagroves TN, Ryan HE, Lu H, Wouters BG, Knapp M, Thibault P, et al. Transcription factor HIF-1 is a necessary mediator of the Pasteur effect in mammalian cells. *Mol Cell Biol* 2001; 21: 3436-3444.

39. Petroff OA, Ogino T, Alger JR. High-resolution proton magnetic resonance spectroscopy of rabbit brain: regional metabolite levels and postmortem changes. *J Neurochem* 1988; 51: 163-171.

40. Stanley JA, Cendes F, Dubeau F, Andermann F, Arnold DL. Proton magnetic resonance spectroscopic imaging in patients with extratemporal epilepsy. *Epilepsia* 1998; 39: 267-273.